Hindawi
Journal of Nanomaterials
Volume 2017, Article ID 4045672, 9 pages
https://doi.org/10.1155/2017/4045672

Research Article

A Novel Poly(3,4-ethylenedioxythiophene)-graphene Oxide/Titanium Dioxide Composites Counter Electrode for Dye-Sensitized Solar Cell

Muhammad Norhaffis Mustafa,[1] Suhaidi Shafie,[2,3] Zulkarnain Zainal,[1,4] and Yusran Sulaiman[1,3]

[1]*Department of Chemistry, Faculty of Science, Universiti Putra Malaysia (UPM), 43400 Serdang, Selangor, Malaysia*
[2]*Department of Electrical and Electronics Engineering, Faculty of Engineering, Universiti Putra Malaysia (UPM), 43400 Serdang, Selangor, Malaysia*
[3]*Functional Device Laboratory, Institute of Advanced Technology, Universiti Putra Malaysia (UPM), 43400 Serdang, Selangor, Malaysia*
[4]*Materials Synthesis and Characterization Laboratory, Institute of Advanced Technology, Universiti Putra Malaysia (UPM), 43400 Serdang, Selangor, Malaysia*

Correspondence should be addressed to Yusran Sulaiman; yusran@upm.edu.my

Received 5 July 2017; Revised 14 August 2017; Accepted 12 September 2017; Published 12 October 2017

Academic Editor: Vincenzo Baglio

PEDOT-based material counter electrodes (CEs) are recently given an enormous attention as new renewable energy sources due to their cost-effectiveness and accessibility, coupled with the simplicity of production. The existing dye-sensitized solar cells (DSSCs) are expensive because they are made using platinum-based glass electrode. In this work, a new CE, that is, poly(3,4-ethylenedioxythiophene)-graphene oxide/titanium dioxide (PEDOT-GO/TiO_2) with a low charge transfer resistance (R_{ct} = 9.0 Ω), was fabricated. In addition, PEDOT-GO/TiO_2 CE possesses a good electrocatalytic activity (ECA) toward the tri-iodide ions reduction and an improved efficiency of 1.166% was reached in DSSC.

1. Introduction

Since the most recent decades, dye-sensitized solar cells (DSSCs) have received great interest, as a substitute toward renewable energies due to the severe energy crisis [1]. A typical DSSC counter electrode (CE) which is platinum (Pt) metal is an expensive metal and thus limits its practical application [2]. Thus, it is critical to find new materials, which are well-appointed for replacing Pt that possesses good electroconductivity and electrocatalytic activity (ECA) toward the reduction of tri-iodide ions and cost-effective [1, 3]. Recently, researchers are interested in the utilization of Pt-free materials such as conducting polymers (CPs) [4], carbon materials [5], and transition metals based inorganic materials [6] as new CE materials in DSSCs due to their remarkable properties that can enhance the efficiency of the solar cell [7]. Poly(3,4-ethylenedioxythiophene) (PEDOT) is a conducting polymer suitable to be utilized as a CE due to its good stability, high electrochemical activity, and excellent transparency [8–10]. Reference [11] reported that PEDOT CE displayed the highest power conversion efficiency (PCE) of 1.35% compared to polypyrrole CE (0.41%) and polythiophene CE (0.49%) due to the fact that PEDOT CE has high ECA and low charge transfer resistance (R_{ct}). In addition, the high surface roughness of PEDOT observed from the FESEM images compared to other polymers also contributed to higher ECA and hence increases the PCE of PEDOT CE [11].

Graphene possesses high carrier mobility [12], high specific surface area [13], excellent thermal conductivity [14],

high optical transparency [15], and high Young's modulus [16]. Reference [17] reported that graphene is a good material to substitute Pt in DSSC because of its outstanding conductivity and high surface area that reduce R_{ct}. However, graphene oxide (GO) CE only yielded a PCE of 0.03% in DSSC due to the low conductivity of GO that leads to a higher series resistance (R_s = 46.5 Ω) [18]. Moreover, good thermal stability, high catalytic activity, and low cost are the reasons why metal oxides are also labeled as potential substitutes for Pt CE [17]. Reference [19] reported that nickel oxide doped Pt as CE yielded a PCE of 3.51%. Another work reported by Zhang et al. [20] reported that incorporation of MnO_2 on PEDOT/GO and PEDOT yielded a higher catalytic activity compared to PEDOT/GO and pure PEDOT.

Herein, we present a new CE that consists of a combination of three different materials which are PEDOT, GO, and TiO_2. The synergistic effect of these materials increases the efficiency of the DSSC. This new CE is Pt-free and does not require high-temperature treatment. It can be simply produced by simple doctor blade technique to coat TiO_2 on ITO followed by deposition of PEDOT-GO onto it. A PCE of 1.166% was obtained for a DSSC with the PEDOT-GO/TiO_2 CE compared to PEDOT (0.015%), TiO_2 (0.001%), PEDOT-GO (0.683%), and Pt (0.727%) CEs. Moreover, PEDOT-GO/TiO_2 CE achieved the lowest R_{ct} value (R_{ct} = 9.0 Ω) compared to other Pt-free CEs.

2. Experimental

2.1. Chemicals and Reagents. 3,4-Ethylenedioxythiophene (EDOT) (stored at 2–4°C), lithium perchlorate ($LiClO_4$), chloroplatinic acid hexahydrate, titanium isopropoxide (TTIP), and titanium dioxide (TiO_2, Degussa P25) were obtained from Sigma Aldrich. Graphene oxide (GO) was purchased from Graphenea and Sigma Aldrich, respectively. Potassium chloride (KCl), acetone, *tert*-butyl alcohol, acetonitrile, and ethanol were obtained from Fisher Chemical, Merck KGaA, J. T. Baker, ChemAR®, and HmbG®, respectively. Ruthenizer 535-bis TBA (N719) and Iodolyte Z-100 were purchased from Solaronix SA. Deionized water from Millipore (Mili- Q, 18.2 MΩ·cm) was utilized throughout the experiments. Indium tin oxide (ITO) glasses (7 Ω/sq) were purchased from Xinyan Technology Ltd.

2.2. Fabrication of TiO_2 Thin Film Photoanode. 2 g of commercial TiO_2 powder (Degussa P25) was mixed with 8 ml of ethanol. The mixture was then stirred until all the TiO_2 powder was dissolved. 0.16 ml TTIP was added to intensify the viscosity of the TiO_2 paste. The mixture was stirred for 30 minutes and proceeded by sonication in an ultrasonic bath for 30 minutes to remove any impurity present. The prepared pastes were coated onto a conductive ITO glass using doctor blade technique. The film was then heated for 2 hours at 100°C using a hot plate. The as-prepared TiO_2 thin film was then cooled. After the cooling process, the photoanode was immersed in the 0.2 mM dye solution of N719 dissolved in the equivalent ratio of acetonitrile: *tert*-butyl alcohol for 24 hours in order for the dye molecules to be fully absorbed. The active area was 0.25 cm^2.

2.3. Fabrication of Platinum, GO, PEDOT, PEDOT-GO, and PEDOT-GO/TiO_2 Counter Electrode. Pt electrode was fabricated by spin coated 50 μL of 0.2 mM chloroplatinic acid hexahydrate on ITO at 1500 rpm for 15 s and was baked at 400°C for 4 hours. The GO CE was prepared by depositing 1 mL of GO (1 mg/mL) on ITO by drop casting whereas PEDOT and PEDOT-GO CEs were prepared potentiostatically at 1.2 V for 100 s with a three-electrode system. The electropolymerization of PEDOT/GO was conducted in an aqueous solution containing 10 mM EDOT and 1 mg/mL GO. For comparison, PEDOT CE was also prepared in 0.1 M $LiClO_4$ without the presence of GO. The silver/silver chloride (Ag/AgCl), TiO_2 coated ITO, and Pt wire were used as a reference, working, and CEs, respectively.

2.4. Characterization Techniques. The electrodeposited CEs were analyzed using Shimadzu XRD Diffractometer with Cu Kα radiation (λ = 1.54 Å) to obtain the crystalline phase of the materials. The scan range was set from 8° to 60°. Each diffractogram was compared to the reference pattern from the Joint Committee on Powder Diffraction Standards (JCPDS). Perkin-Elmer FTIR spectrophotometer coupled with attenuated total reflectance (UATR) accessory was used to identify the functional groups. The surface morphology of the CEs was evaluated using field emission scanning electron microscopy (FESEM, JEOL JSM-7600F). Cyclic voltammetry (CV) and electrochemical impedance spectroscopy (EIS) were used to study the ECA and R_{ct} of the CEs toward the reduction of tri-iodide to iodide. CV measurements were performed using a three-electrode system in a solution containing 1 mM tri-iodide and 0.1 M $LiClO_4$ in acetonitrile. The reference and CE were Ag/Ag^+ and platinum wire, respectively. The potential range applied was −1.0 V to 2.0 V with a scan rate of 0.05 Vs^{-1}. EIS measurements were performed in a dark condition using a two-electrode system at open circuit potential (OCP) with AC amplitude of 0.8 V between the frequency range of 100 kHz and 1 Hz in the presence of Iodolyte Z-100. Tafel polarization measurements were conducted at a scan rate of 10 mVs^{-1}. A symmetric cell containing two identical CEs and an electrolyte Iodolyte Z-100 was used. All electrochemical measurements were carried out using a potentiostat (Autolab PGSTAT204) equipped with NOVA software. Current-voltage measurements were performed using SCS 4200, Keithley Instruments, USA, under 1.5 A.M. (100 $mWcm^{-2}$) irradiation.

3. Results and Discussion

3.1. Fourier Transformed Infrared. Figure 1 shows the FTIR spectra of TiO_2, GO, PEDOT-GO, and PEDOT-GO/TiO_2 CEs. The TiO_2 spectrum shows a band at 545 cm^{-1} which corresponds to the Ti-O-Ti stretching [21]. The peak centered at 936 cm^{-1} belongs to O-Ti-O bonding in anatase TiO_2 [22]. The GO spectrum displays a broad O-H absorption band centered at 3393 cm^{-1} [23]. The peaks at 1717, 1424, 1169, and 1063 cm^{-1} are attributed to the C=O carboxylic group, C-OH deformation, C-O-C, and C-O epoxy, respectively [24]. The FTIR spectrum of PEDOT shows main characteristic

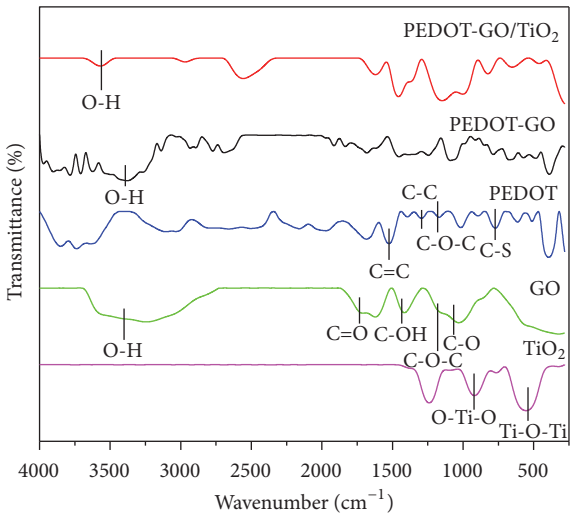

Figure 1: FTIR spectra of TiO_2, GO, PEDOT, PEDOT-GO, and PEDOT-GO/TiO_2.

bands at 1510, 1310, and 1155 cm^{-1} which are attributed to the asymmetric stretching mode of C=C, C-C and the stretching mode of C-O-C, respectively [25]. The C-S bond stretching vibrations in the thiophene ring can be observed at 762 cm^{-1} [26]. The FTIR spectrum of PEDOT-GO shows a combination of GO and PEDOT spectra. All the peaks are seen in PEDOT and GO spectra also present in PEDOT-GO/TiO_2; however, the peaks of TiO_2 (Ti-O-Ti and O-Ti-O bending at 545 and 936 cm^{-1}, resp.) are overlapped with the peak of PEDOT (C-S vibration at 634 cm^{-1}) and GO (C-O epoxy at 838 cm^{-1}).

3.2. Morphological Study. The morphology of PEDOT, GO, TiO_2, PEDOT-GO, and PEDOT-GO/TiO_2 CEs were examined using FESEM. Figure 2(a) shows the FESEM images of electropolymerized PEDOT on ITO glass substrate. The electropolymerized PEDOT shows similar morphology as reported by [27] which is a rough and dense granular shaped morphology was observed. The FESEM image of PEDOT/GO (Figure 2(c)) reveals a uniform wrinkled surface in which resembles paper-like sheet, contributing to an increase in the surface area [28]. This FESEM image is similar to the morphology of GO (Figure 2(b)); however, the wrinkled morphology of PEDOT/GO (Figure 2(c)) is more pronounced than GO (Figure 2(b)) indicating an increase in surface area of the material. As shown in Figure 2(d) the FESEM image of TiO_2 reveals similar morphology as observed by [29] which is porous spherical nanoparticles that is important in the adsorption of the tri-iodide ion. The incorporation of electropolymerized PEDOT-GO onto TiO_2 coated ITO to produce PEDOT-GO/TiO_2 CE (Figure 2(e)) shows a mixture of porous spherical nanoparticles and paper-like sheet morphology. However, the porous spherical nanoparticles morphology of TiO_2 (Figure 2(d)) is more pronounced than PEDOT-GO (Figure 2(c)). This result indicates a synergistic effect of both materials resulting in more active sites being exposed for tri-iodide reduction and subsequently achieving enhanced ECA to yield high PCE.

3.3. XRD Analysis. XRD analysis was performed to examine the crystal structure of GO, TiO_2, PEDOT, PEDOT-GO, and PEDOT-GO/TiO_2 and the XRD patterns are shown in Figure 3. The characteristic peaks at 25.4° (101), 37.9° (004), 48.0° (200), 55.0° (211), 64.5° (204), and 77.7° (215) are associated with the crystal planes of anatase TiO_2 (JCPDS 01-073-1764) [30]. The (001) peak of GO at 10.6° is originated from the stacked graphene sheets in the GO [31]. All conducting polymers show a characteristic peak assigned to the interchain planar ring stacking at approximately 2θ~26° [32–34]. In this work, PEDOT also shows a peak at 25.2° indexed by (107) which is due to interchange planar ring stacking (JCPDS 00-048-1449). PEDOT-GO composite possesses peaks at 10.6° and 24.8°, indicating that PEDOT-GO was successfully deposited on ITO glass whereas PEDOT-GO/TiO_2 which possesses all the peak belongs to anatase TiO_2, stacked graphene sheets of GO, and interchain planar ring stacking of carbon in PEDOT that indicates that all three materials were present in the PEDOT-GO/TiO_2 composite.

3.4. Cyclic Voltammetry. In order to study the ECA properties, CV measurements were carried out and the cyclic voltammograms of platinum, TiO_2, PEDOT, PEDOT-GO, and PEDOT-GO/TiO_2 CEs are shown in Figure 4. A pair of redox peaks was noticed for platinum, PEDOT-GO, and PEDOT-GO/TiO_2 films. The peak in the range 0.75–1.5 V indicates the oxidation of iodide to tri-iodide (see (1)) and the peak in the range of −0.25 to 0.5 V indicates the reduction of tri-iodide to iodide (see (2)).

$$3I^- \longrightarrow I_3^- + 2e^- \quad (1)$$

$$I_3^- + 2e^- \longrightarrow 3I^-. \quad (2)$$

The current densities of two pairs of oxidation and reduction peaks for PEDOT-GO/TiO_2 are higher than PEDOT-GO and platinum, demonstrating excellent electrocatalytic behavior [35]. The reaction rate of the catalyst for the reduction of I_3^- ions in the electrolyte can be influenced by the cathodic peak current density I_{CP} in a CV curve. An enhanced ECA for the catalytic material can be obtained by a higher I_{CP} absolute value. The I_{CP} value of PEDOT-GO/TiO_2 (−5.49 mA·cm^{-2}) is higher than the platinum (−3.57 mA·cm^{-2}) and PEDOT-GO (−3.54 mA·cm^{-2}), suggesting that the ECA toward the I_3^-/I^- redox reaction is greater for PEDOT-GO/TiO_2 compared with PEDOT-GO/TiO_2 and PEDOT-GO. These results are in agreement with R_{ct} obtained from EIS measurements and DSSC with higher efficiency.

3.5. Electrochemical Impedance Spectroscopy. In the DSSCs, the electrolyte of I_3^-/I^- plays a vital role to preserve the regeneration cycle of the electron. The TiO_2 nanoparticles absorb dye molecules and the photon from the sunlight excites the electron of the dye molecules to the CE through an oxidation process. This oxidation process of dye produces a hole in TiO_2; hence, the electrolyte must provide electrons to be transferred back to occupy the holes of TiO_2, which allows

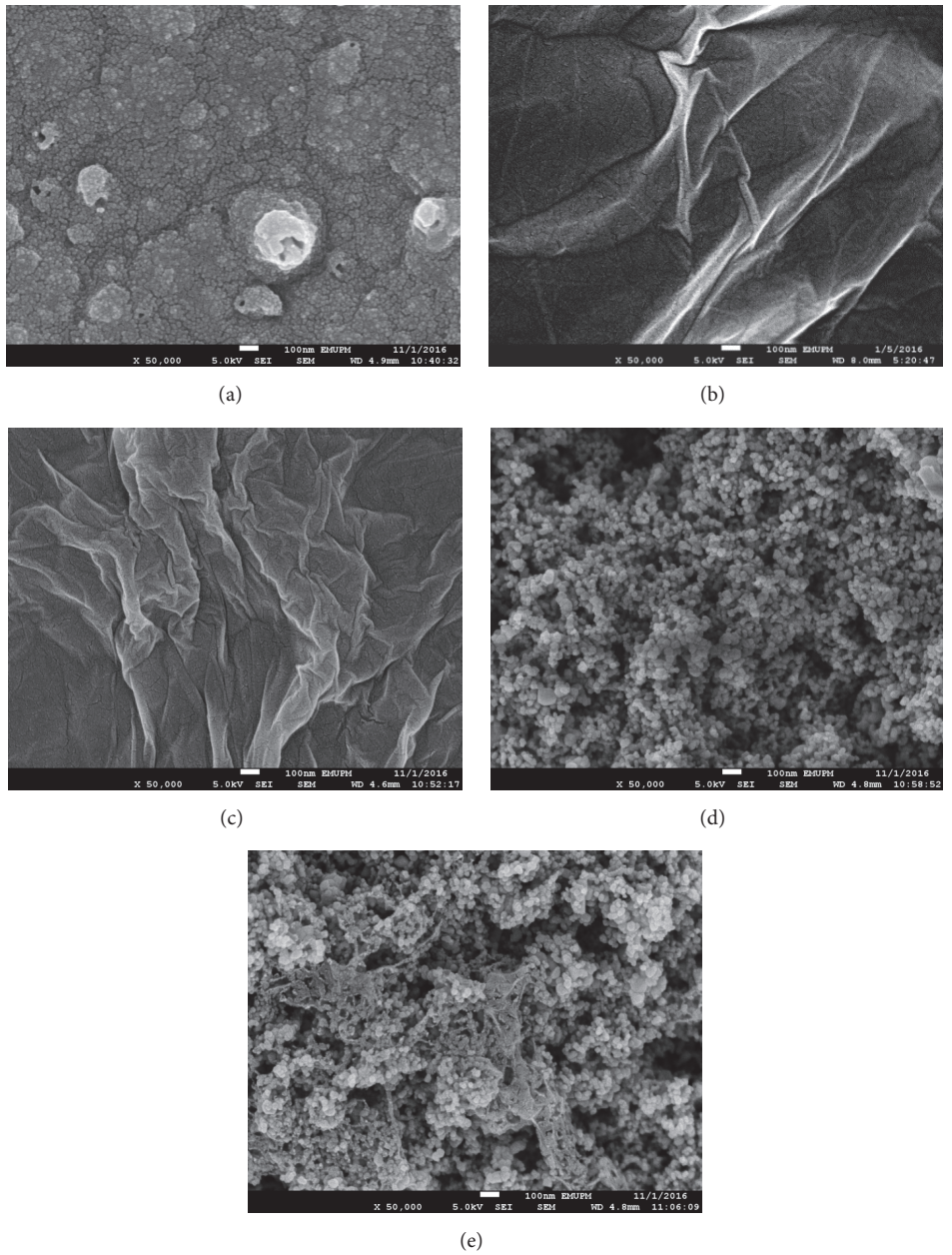

Figure 2: FESEM images of (a) PEDOT, (b) GO, (c) PEDOT-GO, (d) TiO_2, and (e) PEDOT-GO/TiO_2.

the electron of the dye molecule to be generated [36]. Thus, the I_3^- ions should continuously undergo reduction at the CE, as shown in reaction (2). A symmetric cell composed of two identical electrodes was used to perform the EIS analysis in order to study the ohmic series resistance (R_s) of the substrate and its catalytic layer and the charge transfer resistance (R_{ct}) for the reduction of I_3^- at the electrode/electrolyte interface. Figure 5 shows the Nyquist plots of platinum, TiO_2, PEDOT, PEDOT-GO, and PEDOT-GO/TiO_2 CE. The R_s value of PEDOT-GO/TiO_2 (22.2 Ω) is lower than PEDOT-GO (30.6 Ω) and platinum (175.8 Ω), implying better electric conductivity of the former. A smaller value of R_{ct} (9 Ω) is also observed for PEDOT-GO/TiO_2 compared to platinum (19 Ω), indicating good ECA toward the reduction of I_3^- for PEDOT-GO/TiO_2 CE. This result is in agreement with the CV analysis. Figure 6 shows the equivalent circuit used for fitting the Nyquist plots of all CEs. The circuits include the ohmic series resistance (R_s), constant phase element (CPE) that represents the irregularity of sample, and R_{ct}. It was observed that GO has the highest R_{ct} (Table 1) due to the low conductivity followed by TiO_2 and PEDOT. However, after PEDOT is incorporated with GO, the R_{ct} value of PEDOT-GO drops to 21 Ω, indicating faster electron transfer rate due to good charge propagation behavior and low contact resistance [37].

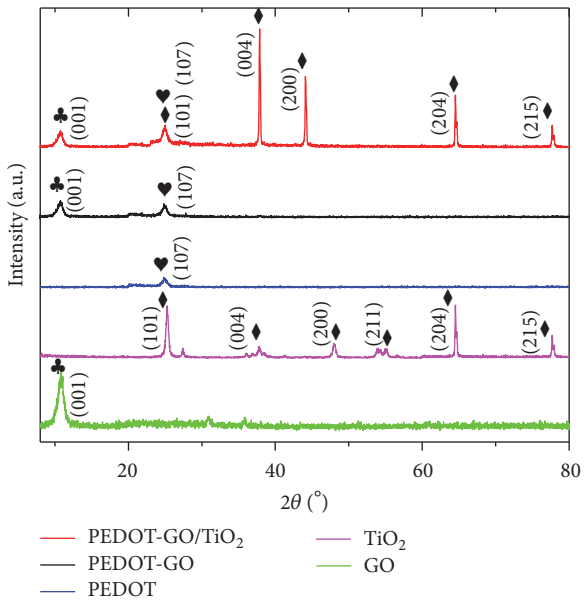

Figure 3: XRD pattern of GO, TiO_2, PEDOT, PEDOT-GO, and PEDOT-GO/TiO_2 CEs. Peaks labeled with "♣," "♦,"and "♥" correspond to the peak of GO, TiO_2 and PEDOT, respectively.

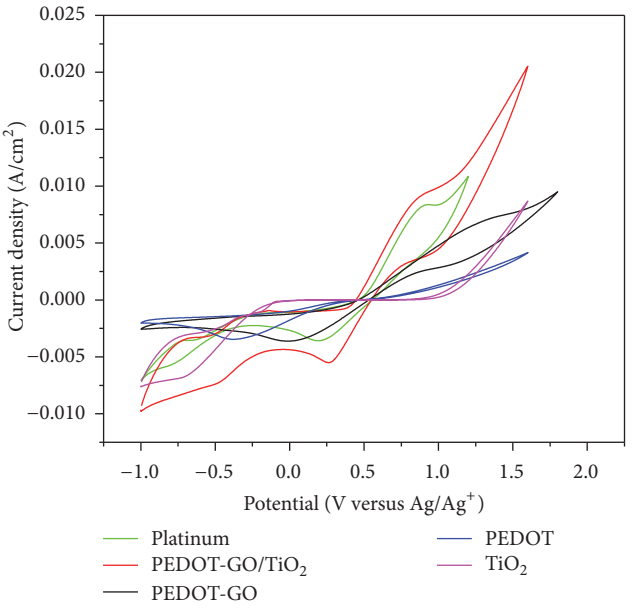

Figure 4: Cyclic voltammetry curves of platinum, TiO_2, PEDOT, PEDOT-GO, and PEDOT-GO/TiO_2 CEs at a scan rate of 50 mVs^{-1} from −1 to +2 V in a solution containing 10 mM LiI, 1 mM I_2, and 0.1 M $LiClO_4$ in acetonitrile solution.

3.6. Photovoltaic Performances of DSSCs. Figure 7 shows the current-voltage (I-V) curves of the DSSC prepared using platinum, TiO_2, PEDOT, PEDOT-GO, and PEDOT-GO/TiO_2 as CEs under AM 1.5 illumination (100 mW/cm^2). The open circuit voltage (V_{oc}), short-circuit current (J_{sc}), maximum power (P_{max}), fill factor (FF), and overall conversion efficiency (η) are summarized in Table 2. Apparently,

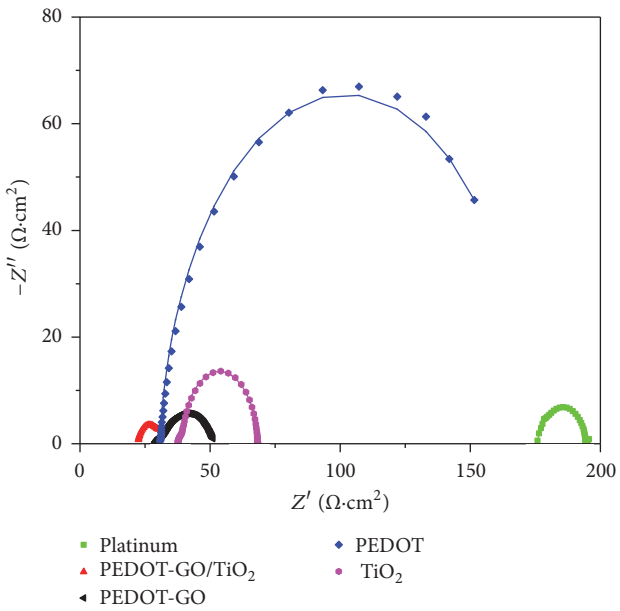

Figure 5: Nyquist plots of DSSCs using platinum, TiO_2, PEDOT, PEDOT-GO, and PEDOT-GO/TiO_2 as CEs. The solid lines represent the fitted data.

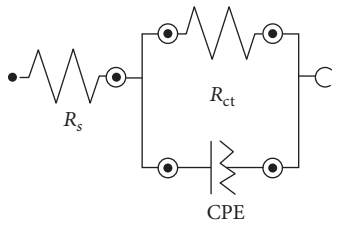

Figure 6: Equivalent circuit of PEDOT-GO/TiO_2 CEs.

Table 1: Impedances data of GO, TiO_2, PEDOT, PEDOT-GO, and PEDOT-GO/TiO_2 as CEs.

CE	R_s (Ω)	R_{ct} (Ω)
GO	44.7	5150
PEDOT	30.7	143
PEDOT-GO	30.6	21
PEDOT-GO/TiO_2	22.2	9
Platinum	175.8	19

TiO_2 CE yielded the lowest power conversion efficiency (PCE) with 0.001% due to slow electron transport and low electron mobility causing recombination process to occur in the electrolyte, hence generating low efficiency [38]. Although PEDOT has excellent conductivity and chemical stability, it also produces a low efficiency (0.015%) that could be due to its small surface area [39] and subsequently resulted in low active site for reduction of iodide to triiodide. In order to overcome this problem a high surface area carbon-based material which is graphene oxide (GO)

Table 2: Photovoltaic performances DSSC based on platinum, TiO_2, PEDOT, PEDOT-GO, and PEDOT-GO/TiO_2 CEs.

CE	J_{sc} (mA/cm^2)	V_{oc} (V)	P_{max} (mW/cm^2)	FF (%)	η (%)
TiO_2	1.728	0.05	0.001	15.28	0.001
PEDOT	1.872	0.30	0.015	26.86	0.015
PEDOT-GO	2.026	0.65	0.683	51.84	0.683
PEDOT-GO/TiO_2	3.967	0.65	1.166	45.22	1.166
Platinum	3.710	0.59	0.727	33.21	0.727

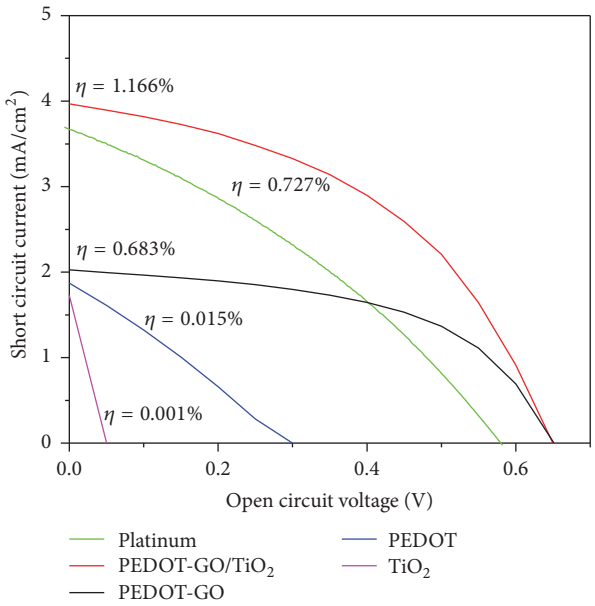

Figure 7: *IV* curves of platinum, TiO_2, PEDOT, PEDOT-GO, and PEDOT-GO/TiO_2 DSSC.

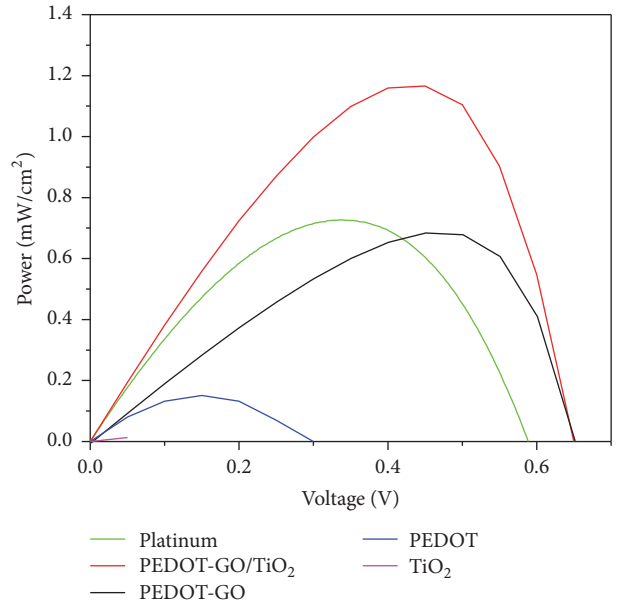

Figure 8: Plot of power and maximum photovoltage (V_{max}) for platinum, TiO_2, PEDOT, PEDOT-TiO_2, and PEDOT-GO/TiO_2 CEs.

is incorporated with PEDOT to form a synergistic effect to obtain a higher efficiency of DSSC [40]. As a result, the PCE of PEDOT-GO CE is enhanced to 0.68%, which is 45.5 times higher than PEDOT CE. In addition, TiO_2 as a source of metal oxide was introduced to PEDOT-GO to increase the performance of DSSC. Even though TiO_2 itself has low efficiency (0.001%), the PCE of TiO_2 incorporated with PEDOT-GO composite gives a promising result with the PCE of 1.166%. The PCE of PEDOT-GO/TiO_2 CE is higher than platinum CE (0.727%) and comparable with conducting polymer based CEs reported in the literature [41, 42]. The novel PEDOT-GO/TiO_2 CE produced in this work is a promising CE due to an enhance PCE observed in PEDOT-GO/TiO_2 CE compared to PEDOT-GO, PEDOT, and TiO_2 CEs. It gives a clear proof that PEDOT-GO/TiO_2 is capable of producing a synergistic effect that utilizes the advantages of each material.

The maximum power densities of CEs are displayed in Figure 8. The J_{max} value can be calculated from the photocurrent-voltage graph based on

$$P = J \cdot V. \quad (3)$$

From the graph, PEDOT-GO-TiO_2 clearly shows the domination on the ability to produce maximum power compared to other CEs which is 1.166 mW/cm^2 due to excellent ECA of PEDOT-GO/TiO_2 toward the reduction of iodide to tri-iodide. The maximum power produced by platinum, PEDOT-GO, PEDOT, and TiO_2 CEs is 0.727, 0.683, 0.015, and 0.001 mW/cm^2, respectively. Due to the high conductivity of PEDOT and high surface area of GO, the maximum power yielded by PEDOT-GO composite is higher than a single compound PEDOT and GO. It is obvious that the maximum power and η of the PEDOT-GO/TiO_2 CE are higher than those of PEDOT-GO CE, which can be corroborated by the data from Tafel polarization curves.

3.7. Tafel Polarization Analysis. Tafel polarization curves were analyzed using the dummy cells to study the interfacial charge transfer behavior of CE/electrolyte and the corresponding results are shown in Figure 9. R_{ct} is inversely proportional to exchange current density (J_o); thus in order to yield a higher J_o a good CE should have lower R_{ct}. J_o can be determined from the intersection of the tangent line of the

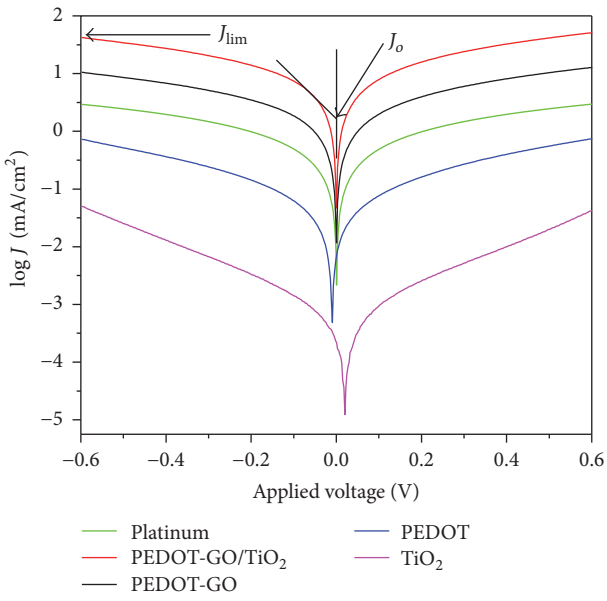

FIGURE 9: Tafel plot of platinum, TiO_2, PEDOT, PEDOT-TiO_2, and PEDOT-GO-TiO_2 CEs.

polarization curve and the extension of the linear segment to the zero bias using [43]

$$J_0 = \frac{RT}{nFR_{ct}}, \quad (4)$$

where R and F are constant, T is the room temperature, and n is the number of electrons involved in the reaction. The limiting diffusion exchange current density (J_{lim}) can also be analyzed from Tafel plot using [44]

$$D = \frac{lJ_{lim}}{2nFC}, \quad (5)$$

where D is the coefficient of tri-iodide, l is the spacer thickness, n is the number of electrons involved in the reduction of tri-iodide at the electrode, F is the Faraday constant, and C is the tri-iodide concentration.

J_{lim} depends on the diffusion coefficient of I^-/I_3^- redox couple. From the Tafel plot, PEDOT-GO/TiO_2 exhibits a higher J_{lim} (1.625 mA/cm^2) compared to PEDOT-GO (1.023 mA/cm^2) and platinum (0.4627 mA/cm^2). A lower J_{lim} value of PEDOT-GO and platinum compared to PEDOT-GO/TiO_2 reveals that PEDOT-GO and platinum have a marginal edge over PEDOT-GO/TiO_2 in terms of improving ECA; nonetheless, PEDOT-GO/TiO_2 CE provides sufficient ECA. J_o values also show a similar trend as of the J_{lim} values where PEDOT-GO/TiO_2, PEDOT-GO, and platinum yielded 0.332, −0.280, and −1.015 mA/cm^2, respectively. A higher J_o reveals that PEDOT-GO/TiO_2 possesses high ECA toward the reduction of tri-iodide to iodide, whereas a higher J_{lim} indicates good contact and better diffusion of electrolyte within the CE [43]. A comparison of the Tafel curves between PEDOT-GO/TiO_2 and PEDOT-GO CEs indicates that the former has a higher catalytic activity compared to the latter. Note that the I^-/I_3^- diffusion capability in the PEDOT-GO/TiO_2 CE is more prominent than that in the PEDOT-GO CE.

4. Conclusion

In summary, a novel PEDOT-GO/TiO_2 CE for DSSC was successfully fabricated using a facile technique. TiO_2 incorporated with PEDOT-GO showed that the electrochemical properties of the final device were affected by catalytic activity layer due to the synergistic effect produced by the combination of three different materials. By applying the PEDOT-GO/TiO_2 composite film as the CE, an efficiency of 1.166% was achieved for the DSSC, which is 58.6% higher than that of a cell based on the PEDOT-GO CE. An excellent enhancement in the conductivity and good electrochemical conductivity for the reduction of I_3^- to I^- were obtained for PEDOT-GO/TiO_2 CE due to the high conductivity of PEDOT, high surface area of GO, and high active area of TiO_2 nanoparticles. Hence, PEDOT-GO/TiO_2 CE is a promising material as a CE for DSSC.

Conflicts of Interest

The authors declare that they have no conflicts of interest.

Acknowledgments

The authors gratefully acknowledge the financial support by the Fundamental Research Grant Scheme (01-02-13-1388FR) from the Ministry of Education Malaysia.

References

[1] I. A. Sahito, K. C. Sun, A. A. Arbab, M. B. Qadir, Y. S. Choi, and S. H. Jeong, "Flexible and conductive cotton fabric counter electrode coated with graphene nanosheets for high efficiency dye sensitized solar cell," *Journal of Power Sources*, vol. 319, pp. 90–98, 2016.

[2] H. Zhou, Y. Shi, D. Qin et al., "Printable fabrication of Pt-and-ITO free counter electrodes for completely flexible quasi-solid dye-sensitized solar cells," *Journal of Materials Chemistry A*, vol. 1, no. 12, pp. 3932–3937, 2013.

[3] G. Calogero, P. Calandra, A. Sinopoli, and P. G. Gucciardi, "Metal nanoparticles and carbon-based nanostructures as advanced materials for cathode application in dye-sensitized solar cells," *International Journal of Photoenergy*, vol. 2010, Article ID 109495, 2010.

[4] H. Kim, G. Veerappan, and J. H. Park, "Conducting polymer coated non-woven graphite fiber film for dye-sensitized solar cells: Superior Pt- and FTO-free counter electrodes," *Electrochimica Acta*, vol. 137, pp. 164–168, 2014.

[5] H. Takada, Y. Obana, R. Sasaki et al., "Improved durability of dye-sensitized solar cell with H2-reduced carbon counter electrode," *Journal of Power Sources*, vol. 274, pp. 1276–1282, 2015.

[6] F. Gong, H. Wang, X. Xu, G. Zhou, and Z.-S. Wang, "In situ gowth of $Co_{0.85}Se$ and $Ni_{0.85}Se$ on conductive substrates as high-performance counter electrodes for dye-sensitized solar cells," *Journal of the American Chemical Society*, vol. 134, no. 26, pp. 10953–10958, 2012.

[7] A. A. Arbab, K. C. Sun, I. A. Sahito, M. B. Qadir, and S. H. Jeong, "Multiwalled carbon nanotube coated polyester fabric as textile based flexible counter electrode for dye sensitized solar cell," *Physical Chemistry Chemical Physics*, vol. 17, no. 19, pp. 12957–12969, 2015.

[8] S. Ahmad, M. Deepa, and S. Singh, "Electrochemical synthesis and surface characterization of poly(3,4-ethylenedioxythiophene) films grown in an ionic liquid," *Langmuir*, vol. 23, no. 23, pp. 11430–11433, 2007.

[9] Y.-H. Ha, N. Nikolov, S. K. Pollack, J. Mastrangelo, B. D. Martin, and R. Shashidhar, "Towards a transparent, highly conductive poly (3,4-ethylenedioxythiophene)," *Advanced Functional Materials*, vol. 14, no. 6, pp. 615–622, 2004.

[10] M. Biancardo, K. West, and F. C. Krebs, "Quasi-solid-state dye-sensitized solar cells: Pt and PEDOT:PSS counter electrodes applied to gel electrolyte assemblies," *Journal of Photochemistry and Photobiology A: Chemistry*, vol. 187, no. 2-3, pp. 395–401, 2007.

[11] M.-H. Yeh, C.-P. Lee, C.-Y. Chou et al., "Conducting polymer-based counter electrode for a quantum-dot-sensitized solar cell (QDSSC) with a polysulfide electrolyte," *Electrochimica Acta*, vol. 57, no. 1, pp. 277–284, 2011.

[12] K. S. Novoselov, A. K. Geim, S. V. Morozov et al., "Electric field in atomically thin carbon films," *Science*, vol. 306, no. 5696, pp. 666–669, 2004.

[13] A. Peigney, C. Laurent, E. Flahaut, R. R. Bacsa, and A. Rousset, "Specific surface area of carbon nanotubes and bundles of carbon nanotubes," *Carbon*, vol. 39, no. 4, pp. 507–514, 2001.

[14] S. Stankovich, D. A. Dikin, G. H. B. Dommett et al., "Graphene-based composite materials," *Nature*, vol. 442, no. 7100, pp. 282–286, 2006.

[15] R. R. Nair, P. Blake, A. N. Grigorenko et al., "Fine structure constant defines visual transparency of graphene," *Science*, vol. 320, no. 5881, p. 1308, 2008.

[16] C. Lee, X. Wei, J. W. Kysar, and J. Hone, "Measurement of the elastic properties and intrinsic strength of monolayer graphene," *Science*, vol. 321, no. 5887, pp. 385–388, 2008.

[17] S. Thomas, T. G. Deepak, G. S. Anjusree, T. A. Arun, S. V. Nair, and A. S. Nair, "A review on counter electrode materials in dye-sensitized solar cells," *Journal of Materials Chemistry A*, vol. 2, no. 13, pp. 4474–4490, 2014.

[18] M.-H. Yeh, L.-Y. Lin, L.-Y. Chang et al., "Dye-sensitized solar cells with reduced graphene oxide as the counter electrode prepared by a green photothermal reduction process," *ChemPhysChem*, vol. 15, no. 6, pp. 1175–1181, 2014.

[19] C.-S. Chou, C.-M. Hsiung, C.-P. Wang, R.-Y. Yang, and M.-G. Guo, "Preparation of a counter electrode with p -type nio and its applications in dye-sensitized solar cell," *International Journal of Photoenergy*, vol. 2010, Article ID 902385, 2010.

[20] L. Zhang, R. Jamal, Q. Zhao, M. Wang, and T. Abdiryim, "Preparation of PEDOT/GO, PEDOT/MnO_2, and PEDOT/GO/MnO_2 nanocomposites and their application in catalytic degradation of methylene blue," *Nanoscale Research Letters*, vol. 10, p. 148, 2015.

[21] S. A. Kazmi, S. Hameed, A. S. Ahmed, M. Arshad, and A. Azam, "Electrical and optical properties of graphene-TiO2 nanocomposite and its applications in dye sensitized solar cells (DSSC)," *Journal of Alloys and Compounds*, vol. 691, pp. 659–665, 2017.

[22] J. C. Yu, L. Zhang, Z. Zheng, and J. Zhao, "Synthesis and characterization of phosphated mesoporous titanium dioxide with high photocatalytic activity," *Chemistry of Materials*, vol. 15, no. 11, pp. 2280–2286, 2003.

[23] W.-K. Zhu, H.-P. Cong, H.-B. Yao et al., "Bioinspired, Ultrastrong, Highly Biocompatible, and Bioactive Natural Polymer/Graphene Oxide Nanocomposite Films," *Small*, vol. 11, no. 34, pp. 4298–4302, 2015.

[24] S. Ye, W. Jin, Q. Huang et al., "Da-KGM based GO-reinforced FMBO-loaded aerogels for efficient arsenic removal in aqueous solution," *International Journal of Biological Macromolecules*, vol. 94, pp. 527–534, 2017.

[25] D. Jacob, P. A. Mini, A. Balakrishnan, S. V. Nair, and K. R. V. Subramanian, "Electrochemical behaviour of graphene-poly (3,4-ethylenedioxythiophene) (PEDOT) composite electrodes for supercapacitor applications," *Bulletin of Materials Science*, vol. 37, no. 1, pp. 61–69, 2014.

[26] T. Abdiryim, A. Ali, R. Jamal, Y. Osman, and Y. Zhang, "A facile solid-state heating method for preparation of poly(3,4-ethelenedioxythiophene)/ZnO nanocomposite and photocatalytic activity," *Nanoscale Research Letters*, vol. 9, no. 1, pp. 1–8, 2014.

[27] J. Rodríguez-Moreno, E. Navarrete-Astorga, F. Martín, R. Schrebler, J. R. Ramos-Barrado, and E. A. Dalchiele, "Semitransparent ZnO/poly(3,4-ethylenedioxythiophene) based hybrid inorganic/organic heterojunction thin film diodes prepared by combined radio-frequency magnetron-sputtering and electrodeposition techniques," *Thin Solid Films*, vol. 525, pp. 88–92, 2012.

[28] H.-C. Tian, J.-Q. Liu, D.-X. Wei et al., "Graphene oxide doped conducting polymer nanocomposite film for electrode-tissue interface," *Biomaterials*, vol. 35, no. 7, pp. 2120–2129, 2014.

[29] K.-W. Lee, M. Kim, J.-M. Kim, J. J. Kim, and I.-H. Lee, "Enhanced photovoltaic performance of back-illuminated dye-sensitized solar cell based on TiO2 nanoparticle/nanowire composite film in cobalt redox system," *Journal of Alloys and Compounds*, vol. 656, pp. 568–572, 2016.

[30] S. Liu, L. Han, Y. Duan et al., "Synthesis of chiral TiO 2 nanofibre with electron transition-based optical activity," *Nature Communications*, vol. 3, article no. 1215, 2012.

[31] T. Chen, Y. Xia, Z. Jia, Z. Liu, and H. Zhang, "Synthesis, characterization, and tribological behavior of oleic acid capped graphene oxide," *Journal of Nanomaterials*, vol. 2014, Article ID 654145, 8 pages, 2014.

[32] Q. Zhao, R. Jamal, L. Zhang, M. Wang, and T. Abdiryim, "The structure and properties of PEDOT synthesized by template-free solution method," *Nanoscale Research Letters*, vol. 9, no. 1, p. 557, 2014.

[33] D. M. Welsh, L. J. Kloeppner, L. Madrigal et al., "Regiosymmetric dibutyl-substituted poly(3,4-propylenedioxythiophene)s as highly electron-rich electroactive and luminescent polymers," *Macromolecules* , vol. 35, no. 17, pp. 6517–6525, 2002.

[34] C. Jiang, G. Chen, and X. Wang, "High-conversion synthesis of poly(3,4-ethylenedioxythiophene) by chemical oxidative polymerization," *Synthetic Metals*, vol. 162, no. 21-22, pp. 1968–1971, 2012.

[35] C.-C. Yang, H. Q. Zhang, and Y. R. Zheng, "DSSC with a novel Pt counter electrodes using pulsed electroplating techniques," *Current Applied Physics*, vol. 11, no. 1, pp. S147–S153, 2011.

[36] J. Wu, Z. Lan, S. Hao et al., "Progress on the electrolytes for dye-sensitized solar cells," *Pure and Applied Chemistry*, vol. 80, no. 11, pp. 2241–2258, 2008.

[37] P. Si, S. Ding, X.-W. Lou, and D.-H. Kim, "An electrochemically formed three-dimensional structure of polypyrrole/graphene nanoplatelets for high-performance supercapacitors," *RSC Advances*, vol. 1, no. 7, pp. 1271–1278, 2011.

[38] K.-P. Wang and H. Teng, "Zinc-doping in TiO_2 films to enhance electron transport in dye-sensitized solar cells under low-intensity illumination," *Physical Chemistry Chemical Physics*, vol. 11, no. 41, pp. 9489–9496, 2009.

[39] D. H. Yoon, S. H. Yoon, K.-S. Ryu, and Y. J. Park, "PEDOT:PSS as multi-functional composite material for enhanced Li-air-battery air electrodes," *Scientific Reports*, vol. 6, Article ID 19962, 2016.

[40] S. Stankovich, D. A. Dikin, R. D. Piner et al., "Synthesis of graphene-based nanosheets via chemical reduction of exfoliated graphite oxide," *Carbon*, vol. 45, no. 7, pp. 1558–1565, 2007.

[41] W. Maiaugree, S. Lowpa, M. Towannang et al., "A dye sensitized solar cell using natural counter electrode and natural dye derived from mangosteen peel waste," *Scientific Reports*, vol. 5, article 15230, 2015.

[42] F. A. Jumeri, H. N. Lim, Z. Zainal, N. M. Huang, A. Pandikumar, and S. P. Lim, "Dual functional reduced graphene oxide as photoanode and counter electrode in dye-sensitized solar cells and its exceptional efficiency enhancement," *Journal of Power Sources*, vol. 293, pp. 712–720, 2015.

[43] M. Chen and L.-L. Shao, "Review on the recent progress of carbon counter electrodes for dye-sensitized solar cells," *Chemical Engineering Journal*, vol. 304, pp. 629–645, 2016.

[44] Y. Liao, K. Pan, L. Wang et al., "Facile synthesis of high-crystallinity graphitic carbon/Fe3C nanocomposites as counter electrodes for high-efficiency dye-sensitized solar cells," *ACS Applied Materials & Interfaces*, vol. 5, no. 9, pp. 3663–3670, 2013.